Proceedings of IMECE2006
2006 ASME International Mechanical Engineering Congress and Exposition
November 5-10, 2006, Chicago, Illinois, USA

IMECE2006-16325

MICROMECHANICS OF HYDROGEN TRANSPORT AND EMBRITTLEMENT IN PIPELINE STEELS

Mohsen Dadfarnia
Department of Mechanical Science and Engineering
158 Mechanical Engineering Building
University of Illinois at Urbana-Champaign
1206 West Green Street
Urbana, IL 61801, USA

Petros Sofronis[1]
Department of Mechanical Science and Engineering
158 Mechanical Engineering Building
University of Illinois at Urbana-Champaign
1206 West Green Street
Urbana, IL 61801, USA

Ian Robertson
Department of Material Science and Engineering
University of Illinois at Urbana-Champaign
1304 West Green Street
Urbana, IL 61801, USA

Brian P. Somerday
Sandia National Laboratories
P. O. Box 969, MS 9403
Livermore, CA 94551, USA

Govindarajan Muralidharan
Oak Ridge National Laboratory
P. O. Box 2008, 1 Bethel Valley Road
Oak Ridge, TN 37831, USA

Douglas Stalheim
DGS Metallurgical Solutions, Inc.
16110 NE 4th Street
Vancouver, WA 98684, USA

ABSTRACT

The technology of large scale hydrogen transmission from central production facilities to refueling stations and stationary power sites is at present undeveloped. Among the problems which confront the implementation of this technology is the deleterious effect of hydrogen on structural material properties, in particular at gas pressure of 1000 psi which is the desirable transmission pressure suggested by economic studies for efficient transport. To understand the mechanisms of hydrogen embrittlement our approach integrates mechanical property testing, TEM observations, and finite element modeling. In this work a hydrogen transport methodology for the calculation of hydrogen accumulation ahead of a crack tip in a pipeline steel is outlined. The approach accounts for stress-driven transient diffusion of hydrogen and trapping at microstructural defects whose density evolves dynamically with deformation. The results are analyzed to correlate the level of load in terms of the applied stress intensity factor with the time after which hydrogen transport takes place under steady state conditions. The transient and steady state hydrogen concentration profiles are used to assess the hydrogen effect on the mechanisms of fracture as they depend on material microstructure.

NOMENCLATURE

b	crack tip opening displacement in the deformed state
b_0	crack tip opening displacement in the undeformed state
c	total hydrogen concentration measured in hydrogen atom per solvent atom
c_0	Initial hydrogen concentration at the absence of any straining
C_0	hydrogen concentration at the crack face
C_L	hydrogen concentration in interstitial sites
C_T	hydrogen concentration in trapping sites
D	hydrogen diffusion coefficient through interstitial sites

1 Corresponding author, Tel. +1-217-333-2636; fax +1-217-244-5707.
Email address: Sofronis@uiuc.edu.

D_{eff} effective hydrogen diffusion coefficient
D_{ij}^{e} elastic part of deformation rate tensor
D_{ij}^{p} plastic part of deformation rate tensor
D_{ij}^{h} deformation rate for lattice straining due to hydrogen
D_{ij} $= D_{ij}^{e} + D_{ij}^{p} + D_{ij}^{h}$, total deformation rate
E Young's modulus
G shear modulus
h slope of uniaxial Cauchy stress vs logarithmic plastic strain
K_I stress intensity factor
K_T equilibrium constant
L domain size
L_{nd} non-dimensionalizing length
n work hardening coefficient
N_A Avogadro's number
N_T trap density
N_L number of solvent atoms per unit volume
R universal gas constant
t time
t_{ss} effective time to steady state
T temperature
V_H partial molar volume of hydrogen
V_M molar volume of the host lattice
W_B Trap binding energy
x_i coordinate system
α number of sites per trap
β number of NILS per host atom
δ_{ij} Kronecker delta
Δv $= V_H / N_A$, volume increase per hydrogen atom
ε_0 yield strain
ε^p equivalent plastic strain
θ_L occupancy of the interstitial sites
θ_T occupancy of the trapping sites
ν Poisson's ratio
ξ_i $= x_i / L_{nd}$, non-dimensional coordinate
ρ $= \sigma_{kk} V_H / 3RT$
σ_0 yield stress
σ_e equivalent stress
σ_{ij} Cauchy's stress
σ'_{ij} devioteric stress
$\overset{\nabla}{\sigma}_{ij}$ Jaumann rate of stress
Ω mean atomic volume of the host lattice
τ $= Dt / L_{nd}^{2}$, non-dimensional time
ϕ $= C_L / C_0$, non-dimensional NILS concentration

INTRODUCTION

The deleterious effect of hydrogen on the fracture behavior of iron and steels has been known for long time [1]. In the presence of hydrogen, materials fail at very low load levels relative to those they can sustain in the absence of hydrogen (e.g. see [2] and [3]). It was thought previously that hydrogen embrittlement occurs only in high strength steels, with the effect becoming weaker as the strength reduces. That is certainly true at high strengths but not always true for the medium or low-strength steels [4]. Low- to medium-strength steels, depending on their composition and microstructure, are also susceptible to hydrogen embrittlement. These types of steels are normally used in pipeline and storage vessels for their low cost, particularly in pipelines, where many miles of structure are often involved.

Hydrogen transport is one of the important aspects of hydrogen embrittlement. Hydrogen atoms after adsorption and absorption move into the lattice to the sites where degradation occurs. As Birnbaum [5] pointed out, the ductility dependence on temperature and strain rate, the incubation period and the critical hydrogen concentration build-up before fracture reflect the hydrogen transport kinetics rather than the mechanisms of failure. Therefore, the analysis of the hydrogen transport processes should precede any attempt to address the issue of hydrogen embrittlement related failure [6].

The first attempt to couple nonlinear diffusion phenomena with elastoplastic deformation ahead of a crack tip was made by Kitagawa and Kojima [7]. Considering drift due to hydrostatic stress and trapping generated by plastic deformation, Sofronis and McMeeking [8] studied transient diffusion of hydrogen and hydrogen trapping at microstructural defects in iron and steel in the area around a blunting crack tip. Lufrano and Sofronis [9] extended the model of Sofronis and McMeeking by including the effect of hydrogen induced dilatation on the material constitutive model, and analyzed the interaction of hydrogen with local plasticity at cracked and round-notched geometries. In systems with large hydrogen solubility, the dilatational effect of hydrogen becomes important at high hydrogen concentrations as it affects both the stress relaxation and the diffusion paths. Krom [10] extended the model of Sofronis and McMeeking by introducing a strain rate factor in the diffusion equation to accurately account for the hydrogen balance in normal interstitial lattice sites (NILS) and trapping sites. This strain rate factor is particularly important in transient calculations of hydrogen at high strain rates. Using this modified transport model, Taha and Sofronis [11] extended the analysis of Lufrano and Sofronis [9] to assess embrittlement in both low and high strength materials.

In all studies above, a uniform non-zero initial hydrogen concentration in NILS was assumed throughout the material before loading. This type of initial condition pertains to specimens which are first charged and then tested. However, it does not represent the case of a cracked specimen strained in hydrogen gas while hydrogen diffuses in the specimen though the crack faces. This latter case represents a real-world scenario of hydrogen ingress through a flaw in the interior wall of a

pipeline. For such a situation, it is assumed that the bulk of the specimen is hydrogen free and the crack faces are at an equilibrium concentration as dictated by Sievert's law. The purpose of this study is to correlate the steady state values for the hydrogen concentration with the applied loads and the geometric characteristics of a cracked specimen charged in a hydrogen gas environment. Such results may be used to predict an upper bound to the time required for the embrittlement of a pipeline steel by hydrogen.

The above brief outline of the hydrogen embrittlement phenomena and the finite element simulation methodology to be presented in the Problem Statement and Elastoplastic Deformation in the Presence of Hydrogen sections that follow are the same as those of a previous paper on the subject by the same authors [12]. The remainder of the paper is organized as follows: The system description and mathematical modeling issues of the coupled hydrogen diffusion and elasto-plastic problem are explained in the next two sections. Numerical results for diffusion of hydrogen under small scale yielding conditions are presented at various levels of applied stress intensity factor. A scaling of the steady state hydrogen concentration profile is identified with the applied loads. This result is used for the calculation of the time it takes for the hydrogen profiles to reach steady state in terms of the domain size.

PROBLEM STATEMENT

The hydrogen atom due to its small size can easily diffuse into metals and alloys. The hydrostatic stress and plastic deformation induce drift in concentration [8]. Solution of hydrogen into the lattice causes lattice dilatation [13] and affects the material properties [14]. Therefore, hydrogen diffusion and material elastoplasticity is a coupled problem.

Hydrogen Transport

Hydrogen is assumed to reside either at normal interstitial lattice sites (NILS) or reversible trapping sites at microstructural defects such as internal intefaces or dislocations generated by plastic deformation [8,11]. The two populations are always in equilibrium according to Oriani's theory [15] such that

$$\frac{\theta_T}{1-\theta_T} = \frac{\theta_L}{1-\theta_L} K_T, \quad K_T = \exp\left(\frac{W_B}{RT}\right) \tag{1}$$

where θ_L is occupancy of the interstitial sites, θ_T is occupancy of the trapping sites, W_B is the trap binding energy, R = 8.314 J/mole K is the universal gas constant, and T is the absolute temperature. The hydrogen concentration in trapping sites C_T, measured in hydrogen atoms per unit volume, can be written as

$$C_T = \theta_T \alpha N_T, \tag{2}$$

where α denotes the number of sites per trap, and $N_T = N_T(\varepsilon^p)$ denotes the trap density in number of traps per unit volume as a function of the amount of the local plastic deformation. The hydrogen concentration in interstitial sites C_L, measured in hydrogen atoms per unit volume, can be stated as

$$C_L = \theta_L \beta N_L \tag{3}$$

where β denotes the number of NILS per solvent atom, N_L denotes the number of solvent atoms per unit volume given by

$$N_L = \frac{N_A}{V_M} \tag{4}$$

with $N_A = 6.0232 \times 10^{23}$ atoms per mole being Avogadro's number, and V_M is the molar volume of the host lattice measured in units of volume per mole.

Using Eqs. (1) - (3), one can cast the governing equation for transient hydrogen diffusion accounting for trapping and hydrostatic drift as [8,10]

$$\frac{D}{D_{eff}}\frac{dC_L}{dt} + \alpha\theta_T \frac{dN_T}{d\varepsilon^p}\frac{d\varepsilon^p}{dt} - DC_{L,ii} + \left(\frac{DV_H}{3RT} C_L \sigma_{kk,i}\right)_{,i} = 0, \tag{5}$$

where $()_{,i} = \partial()/\partial x_i$, d/dt is the time derivative, D is the hydrogen diffusion coefficient through NILS, D_{eff} is an effective diffusion coefficient given by

$$\frac{D_{eff}}{D} = \left(1 + \frac{\partial C_T}{\partial C_L}\right)^{-1}, \tag{6}$$

V_H is the partial molar volume of the hydrogen in solid solution, σ_{ij} is the Cauchy stress, and a repeated index implies the standard summation convention over the range. Eqn. (5) shows that in order to calculate the hydrogen distribution within a solid, one should solve a coupled problem of hydrogen diffusion and elastoplasticity.

Using Eqs. (1) - (3), one can write C_T in terms of C_L as

$$C_T = \frac{K_T \alpha N_T C_L}{\beta N_L + (K_T - 1) C_L}, \tag{7}$$

and therefore from Eqn. (6) one finds

$$\frac{D}{D_{eff}} = 1 + \frac{K_T \alpha \beta N_L N_T}{[\beta N_L + (K_T - 1) C_L]^2}. \tag{8}$$

The Oriani's model assumes that the trap filling kinetics is very rapid. Consequently, the effective diffusion coefficient D_{eff} is less than the normal NILS diffusion coefficient D as long as the traps are not saturated or as new traps are created by plastic straining.

Consider the following non-dimensional parameters

$$\xi_i = \frac{x_i}{L_{nd}}, \tau = \frac{Dt}{L_{nd}^2}, \phi = \frac{C_L}{C_0}, \rho = \sigma_{kk}\left(\frac{V_H}{3RT}\right), \tag{9}$$

where L_{nd} is a non-dimensionalizing length which can be chosen equal to the initial domain size L, and C_0 is a constant hydrogen concentration. Introducing the non-dimensional parameters in Eq. (5), one can rewrite the hydrogen transport equation as

$$\frac{D}{D_{eff}}\frac{d\phi}{d\tau}+\frac{\alpha\theta_T}{C_0}\frac{dN_T}{d\varepsilon^p}\frac{d\varepsilon^p}{d\tau}-\frac{\partial^2\phi}{\partial\xi_i\partial\xi_i}+\frac{\partial}{\partial\xi_i}\left(\phi\frac{\partial\rho}{\partial\xi_i}\right)=0. \quad (10)$$

ELASTOPLASTIC DEFORMATION IN THE PRESENCE OF HYDROGEN

The material is assumed to be linearly elastic and isotropic with moduli and flow stress independent of the local hydrogen concentration. In the plastic regime, the material hardens isotropically and flows according to von-Mises J_2 flow theory. In the case of finite deformation in the presence of hydrogen, the associated flow rule for plastic loading is given by

$$\overset{\nabla}{\sigma}_{ij} = 2G\left(\delta_{ik}\delta_{jl}+\frac{\nu}{1-2\nu}\delta_{ij}\delta_{kl}-\frac{3\sigma'_{ij}\sigma'_{kl}}{2\left(\frac{h}{3G}+1\right)\sigma_e{}^2}\right)\left(D_{kl}-D^h_{kl}\right), \quad (11)$$

and for deformation in the elastic regime by

$$\overset{\nabla}{\sigma}_{ij} = 2G\left(\delta_{ik}\delta_{jl}+\frac{\nu}{1-2\nu}\delta_{ij}\delta_{kl}\right)\left(D_{kl}-D^h_{kl}\right), \quad (12)$$

where D_{ij} denotes the total deformation rate tensor and equals the symmetric part of the velocity gradient in spatial coordinates, δ_{ij} is the Kronecker delta, the superscript ∇ denotes the Jaumann stress rate, $\sigma'_{ij}=\sigma_{ij}-\sigma_{kk}/3\,\delta_{ij}$ is the devioteric stress, $\sigma_e=\sqrt{3\sigma'_{ij}\sigma'_{ij}/2}$ is the equivalent stress, G and ν are the shear modulus and Poisson's ratio respectively, and $h=d\sigma_e/d\varepsilon^p$ is the slope of the uniaxial Cauchy stress vs logarithmic plastic strain ε^p. In multiaxial deformation, ε^p is defined as $\varepsilon^p=\sqrt{2D^p_{ij}D^p_{ij}/3}$. The total deformation rate D_{ij} can be expressed as

$$D_{ij}=D^e_{ij}+D^p_{ij}+D^h_{ij} \quad (13)$$

where D^e_{ij}, D^p_{ij}, and D^h_{ij} denote the elastic, plastic, and hydrogen parts, respectively. The mechanical effect of the hydrogen solute atoms is purely dilatational [13] and is phrased in terms of the deformation rate as

$$D^h_{ij}=\frac{d}{dt}\left[\ln\left(1+\frac{(c-c_0)\Delta v}{3\Omega}\right)\right]\delta_{ij}, \quad (14)$$

where c is total hydrogen concentration measured in hydrogen atoms per solvent atom, c_0 is the initial hydrogen concentration in the stress free lattice, $\Delta v = V_H/N_A$ is the volume increase per hydrogen atom introduced into solution, and Ω is the mean atomic volume of the host metal atom.

The hydrogen diffusion initial/boundary-value problem and the elastic-plastic boundary problem are coupled [8]. The finite element procedures for the solution of the coupled problems are outlined in the works by Sofronis and McMeeking [8] and Lufrano *et al*. [16].

NUMERICAL RESULTS

In this section, the initial/boundary-value problem of hydrogen diffusion coupled with material elastoplasticity is solved near a blunting crack tip. Plain strain conditions are assumed at temperature of 300 K. The boundary approach of small scale yielding under mode I opening is used to analyze an infinite body with a semi-infinite crack of initial crack tip opening displacement of b_0. Since the plastic zone is confined in the area near the crack tip and its size is much smaller than the dimensions of the domain, one can consider a finite geometry domain with the asymptotic displacement boundary conditions of the Irwin singular linear elastic field [17] imposed on the boundary far away from the crack tip. Figure 1 shows the geometry and boundary conditions of the problem. The chosen shape of the outer boundary allowed for convenient and very fine element discretization of the part of the domain close to the crack face. Such fine discretization was required for the treatment of the steep concentration gradients set by the imposed hydrogen concentration boundary condition at the crack face. The distance *L* is set equal to 14.3 mm and the initial crack opening displacement b_0 equal to 6 μm.

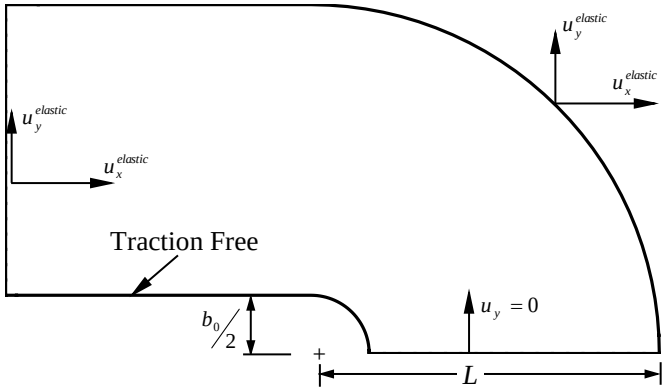

FIGURE 1: DESCRIPTION OF BOUNDARY CONDITIONS FOR THE ELASTOPLASTIC PROBELM AT A BLUNTING CRACK TIP. THE PARAMETER b_0 DENOTES THE CRACK OPENING DISPLACEMENT IN THE UNDEFORMED STATE, AND $u_x^{elastic}$ AND $u_y^{elastic}$ ARE THE ASYMPTOTIC DISPLACEMENTS OF IRWIN'S SINGULAR FIELD [17] IN X- AND Y-DIRECTION, RESPECTIVELY.

It is assumed that there is no hydrogen in the material at time zero. The displacement is applied incrementally at a constant stress intensity factor rate toward a final value K_I. Since the plasticity of the material is rate independent, the response of the system is independent of the loading rate. Then, while the load is kept fixed at K_I, hydrogen diffusion through the crack faces is switched on. It should be mentioned that T-stress effects on the interaction of hydrogen with the material microstructure ahead of a crack tip are also important, in particular in the case of shallow cracked specimens as Liang *et*

al. [18] have found. The interaction of the T-stress with the hydrogen transport under the boundary conditions outlined in Fig. 1 is the subject of a subsequent investigation.

The boundary and initial conditions for the NILS concentration is shown in Fig. 2. The NILS hydrogen concentration on the crack surface is assumed to be in equilibration with hydrogen gas at pressure of 1 atm. Therefore, a constant NILS concentration boundary condition, $C_L = C_0 = 2.084\times10^{21}$ H atoms/m^3 ($= 2.46\times10^{-8}$ H atoms per solvent atoms) is enforced on the crack surface at all times. The outer surface is assigned a zero concentration boundary condition, i.e. $C_L = 0$, and zero flux is prescribed along the axis of symmetry ahead of the crack tip.

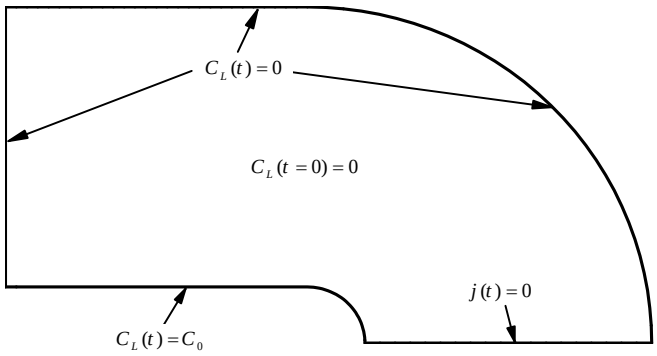

FIGURE 2: DESCRIPTION OF INITIAL AND BOUNDARY CONDITIONS FOR THE DIFFUSION PROBLEM AT THE BLUNTING CRACK TIP. THE PARAMETER C_0 IS NILS HYDROGEN CONCENTRATION AT THE CRACK FACE AND *j* IS THE HYDROGEN FLUX IN Y-DIRECTION.

TABLE 1. MATERIAL PROPERTIES

Properties	Symbol	Value
Young's modulus	E	201.88 GPa
Poisson's ratio	ν	0.3
Yield stress	σ_0	595 MPa
Work hardenning exponent	n	0.059
Number of sites per trap	α	1
Number of NILS per host atom	β	1
Trap binding energy	W_B	60 KJ/mole
Molar volume of the metal	V_M	7.116 cm^3/mole
Partial molar volume of H	V_H	2 cm^3/mole
Diffusion coefficient	D	2×10^{-11} m^2/s
Volume change per H atom	$\Delta v/\Omega$	0.281

The material used in the simulation is a new X70/X80 type of an acicular ferrite pipeline microstructure whose properties are given in Table 1. The uniaxial stress-strain curve has been measured experimentally and is given by a power-law relationship of the form $\sigma_e = \sigma_0(1+\varepsilon^p/\varepsilon_0)^n$, where ε^p is plastic strain and $\varepsilon_0 = \sigma_0/E$. The trap density N_T is assumed to increase with plastic straining according to the experimental results of Kumnick and Johnson [19] who also found a trap binding energy of 60 KJ/mol.

Figures 3 and 4 show contour plots of normalized hydrostatic stress and plastic strain, respectively, at a stress intensity factor of K_I =70 MPa$\sqrt{\text{m}}$. The corresponding crack tip opening displacement b was equal to 25.03 μm, about 4 times the initial crack tip opening displacement b_0. As it can be seen in Fig. 4, the plastic zone is small compared to the size of the domain and the assumption of small scale yielding is valid.

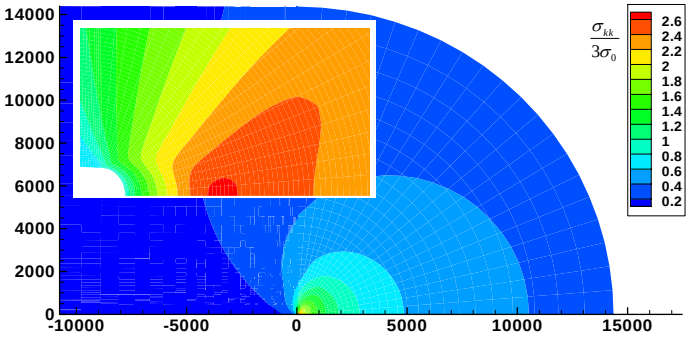

FIGURE 3: CONTOUR PLOT OF NORMALIZED HYDROSTATIC STRESS $\sigma_{kk}/3\sigma_0$ AT $K_I = 70$ MPa$\sqrt{\text{m}}$. THE INSET SHOWS THE HYDROSTATIC STRESS NEAR THE NOTCH ROOT AND DIMENSIONS ARE IN MICRONS.

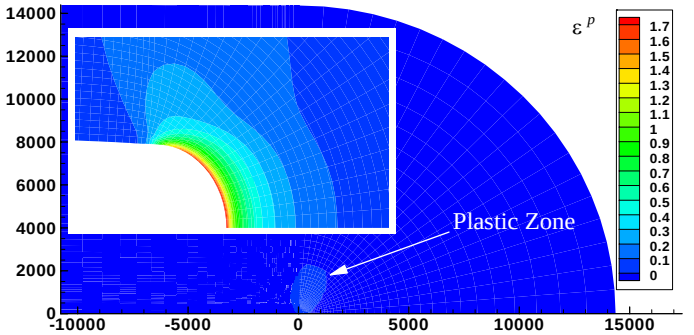

FIGURE 4: CONTOUR PLOT OF EQUIVALENT PLASTIC STRAIN ε^p AT $K_I = 70$ MPa$\sqrt{\text{m}}$. THE INSET SHOWS THE EQUIVALENT PLASTIC STRAIN NEAR THE CRACK ROOT AND DIMENSIONS ARE IN MICRONS.

The distribution of hydrogen concentration reached a steady state after *t* = 170 days, where *t* = 0 corresponds to the switching on of hydrogen diffusion. The contour plots of the hydrogen field parameters at steady state are shown in Figs. 5-7.

Figure 5 shows the normalized NILS concentration C_L / C_0 at steady state. The distribution of C_L near the crack root varies in accordance with the hydrostatic stress (inset of Fig. 3).

The equivalent plastic strain attains its peak value at the crack root and rapidly decreases at distances away from the root. Thus, as Fig. 6 shows, the site of accumulation of trapped hydrogen is near the crack surface and the profile of the trapped concentration C_T follows closely that of the plastic strain (Fig.

4). This is because the trap density increases monotonically with plastic strain [19]. Figure 7 shows the normalized total hydrogen concentration in the domain which is essentially governed by the trap populations (Fig. 6) due to the smaller magnitude of hydrogen concentration in NILS.

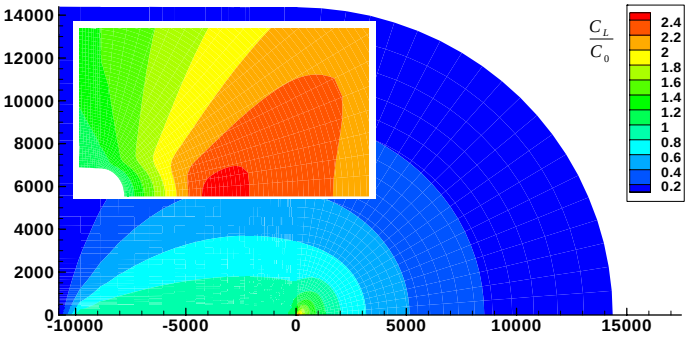

FIGURE 5: CONTOUR PLOT OF NILS HYDROGEN CONCENTRATION C_L/C_0 AT STEADY STATE UNDER $K_I = 70$ MPa$\sqrt{\text{m}}$. THE INSET SHOWS THE CONCENTRATION AT THE CRACK ROOT.

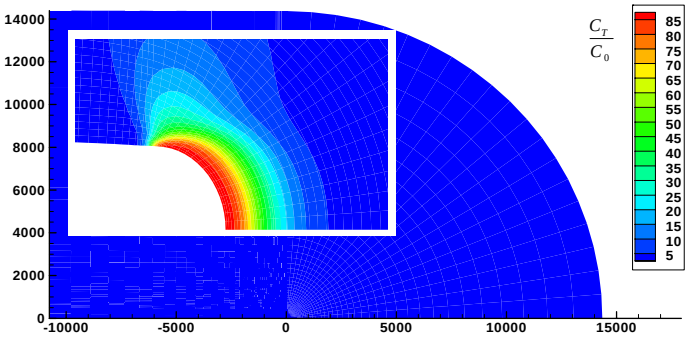

FIGURE 6: CONTOUR PLOT OF HYDROGEN CONCENTRATION AT TRAPPING SITES C_T/C_0 AT STEADY STATE FOR UNDER $K_I = 70$ MPa$\sqrt{\text{m}}$. THE INSET SHOWS HYDROGEN CONCENTRATION AT THE CRACK ROOT.

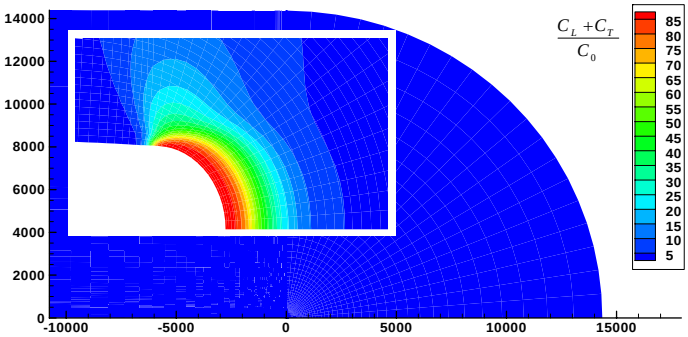

FIGURE 7: CONTOUR PLOT OF TOTAL HYDROGEN CONCENTRATION $(C_L + C_T)/C_0$ AT STEADY STATE UNDER $K_I = 70$ MPa$\sqrt{\text{m}}$. THE INSET SHOWS HYDROGEN CONCENTRATION AT THE CRACK ROOT.

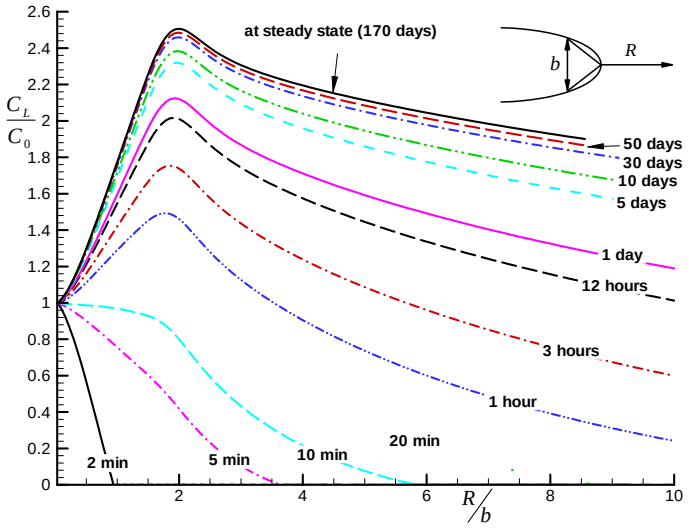

FIGURE 8: EVOLUTION OF NORMALIZED HYDROGEN CONCENTRATION C_L/C_0 IN NILS VS NORMALIZED DISTANCE R/b AHEAD OF THE CRACK TIP AT $K_I = 70$ MPa$\sqrt{\text{m}}$. THE PARAMETER $b = 25.03$ μm DENOTES THE CURRENT CRACK TIP OPENING DISPLACEMENT.

Figure 8 shows the normalized concentration C_L/C_0 in NILS at different times against normalized distance *R/b* from the notch root in the undeformed configuration. The parameter *b* denotes the current crack tip opening displacement at $K_I = 70$ MPa$\sqrt{\text{m}}$ and is defined by the 90˚ intersection method. The effect of hydrostatic stress on configuring the steady state hydrogen concentration profile in NILS can be clearly seen in this figure.

The shape of the NILS concentration profile is dictated by several processes. The high value of the hydrogen concentration gradient at the crack surface forces hydrogen to diffuse into the specimen. At the root of the crack notch, the large number of trap sites generated by plastic straining demands for hydrogen. At the same time, hydrogen is attracted to the hydrostatic peak location inside from the root. Due to the large trap binding energy, trapping sites are filled up quickly depleting hydrogen from the NILS. After the trapping sites are saturated, hydrostatic stress gradients pull hydrogen away from the crack tip toward the hydrostatic stress peak location, and this creates a local peak in the NILS hydrogen concentration. This process along with the fact that the concentration C_L at the crack surface is kept constant at the value C_0 at all times determines the shape of the C_L concentration profiles, as shown in Fig. 8.

In order to investigate the effect of the magnitude of the applied load on the evolution of the hydrogen concentration profiles, additional simulations were carried out at different applied stress intensity factors K_I. Specifically, $K_I = 55$ and 80 MPa$\sqrt{\text{m}}$ were used. The small scale yielding requirement under these loads is satisfied and the crack tip opening

displacements are $b =$ 18.13 μm ($\approx 3b_0$) and 30.16 μm ($\approx 5b_0$), respectively for $K_I = 55$ and 80 MPa$\sqrt{\text{m}}$.

Figures 9 and 10 show the evolution of the normalized concentration C_L/C_0 profiles in terms of the normalized distance *R/b* from the crack tip under stress intensity factors of 55 and 80 MPa$\sqrt{\text{m}}$, respectively.

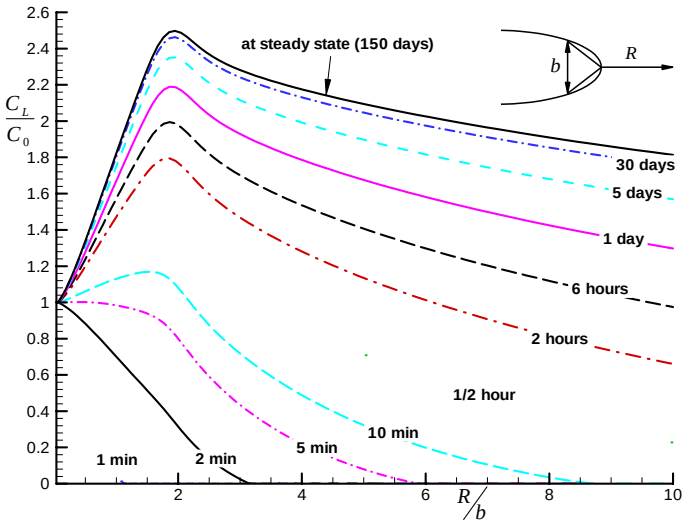

FIGURE 9: EVOLUTION OF THE NORMALIZED HYDROGEN CONCENTRATION C_L/C_0 IN NILS VS. NORMALIZED DISTANCE R/b AHEAD OF THE CRACK TIP UNDER $K_I = 55$ MPa$\sqrt{\text{m}}$. THE PARAMETER $b = 18.13$ μm DENOTES THE CURRENT CRACK TIP OPENING DISPLACEMENT.

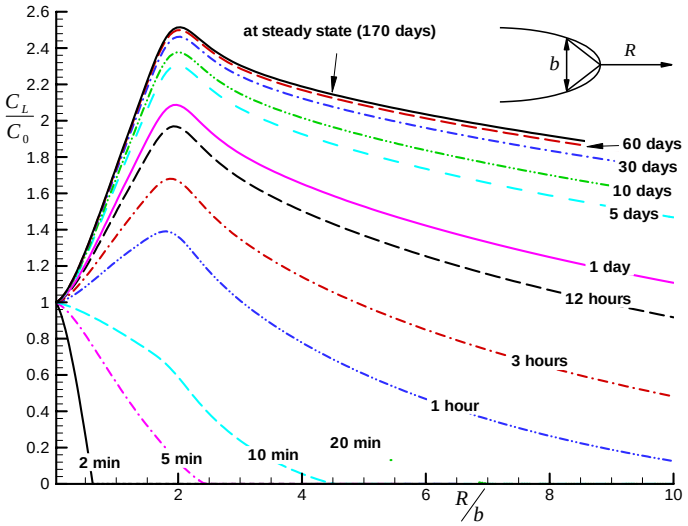

FIGURE 10: EVOLUTION OF THE NORMALIZED HYDROGEN CONCENTRATION C_L/C_0 IN NILS VS. NORMALIZED DISTANCE R/b AHEAD OF THE CRACK TIP UNDER $K_I = 80$ MPa$\sqrt{\text{m}}$. THE PARAMETER $b = 30.16$ μm DENOTES THE CURRENT CRACK TIP OPENING DISPLACEMENT.

Clearly, Figs. 8-10 show that for all cases of applied stress intensity factor the time to steady state is about 170 days and the corresponding shapes of the curves are nearly the same. Certainly, the curves are not the same at the earlier times (e.g. 2 or 10 min) of hydrogen diffusion, but for the times close to the steady state, they do look the same. The parameter t_{ss} is defined to denote the time at which the NILS hydrogen concentration at the peak location reaches 98% of the final steady state value. Figure 11 shows the time t_{ss} plotted as a function of the applied stress intensity factor. The plot shows that t_{ss} is independent of the magnitude of the applied stress intensity factor and equal to 30 days.

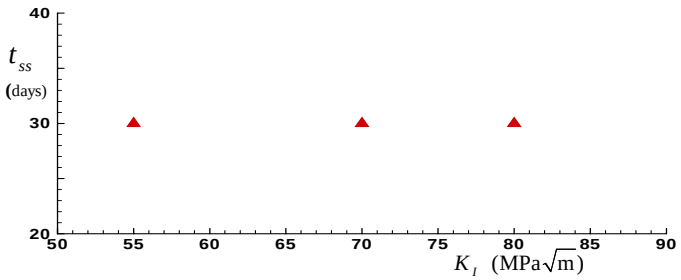

FIGURE 11: PLOT OF t_{ss} VS. THE APPLIED STRESS INTENSITY FACTOR K_I FOR A DOMAIN WITH $L = 14.3$mm. THE PARAMETER t_{ss} DENOTES TIME IT TAKES FOR THE NILS CONCENTRATION AT THE PEAK LOCATION TO REACH 98% OF ITS STEADY STATE VALUE.

DISCUSSION

An effective time t_{ss} of hydrogen diffusion toward steady state has been introduced for expediency in our finite element simulations. Figure 12 shows the profiles of NILS hydrogen concentration ahead of the crack tip at $t_{ss} = 30$ days under three representative magnitudes of the applied stress intensity factor for a domain size of $L = 14.3$mm. Clearly, the profile at time t_{ss} scales with R/b. This scaling of the profiles which can be generalized for any domain size L can be explained by the steady state form of the normalized hydrogen transport Eq.(10):

$$-\frac{\partial^2 \phi}{\partial \xi_i \partial \xi_i} + \frac{\partial}{\partial \xi_i}\left(\phi \frac{\partial \rho}{\partial \xi_i}\right) = 0. \qquad (15)$$

If one considers that the non-dimensionalizing length L_{nd} is equal to b, $\partial\rho/\partial\xi_i$ is a function of ξ_i with no explicit dependence on K_I. Therefore, the solution for ϕ *near the crack tip* is a function of ξ_i with no explicit dependence on K_I. Attention should be drawn to the fact that even though form (15) is the same for all applied stress intensities, the condition $\phi = 0$ in the solution process on the outer boundary of the domain is applied at $\xi_i = x_i/b$ which is dependent on K_I because so is b. It should be mentioned that the scaling of the normalized hydrogen concentration as shown in Fig. 12 holds

for any value of the stress intensity factor under small scale yielding conditions.

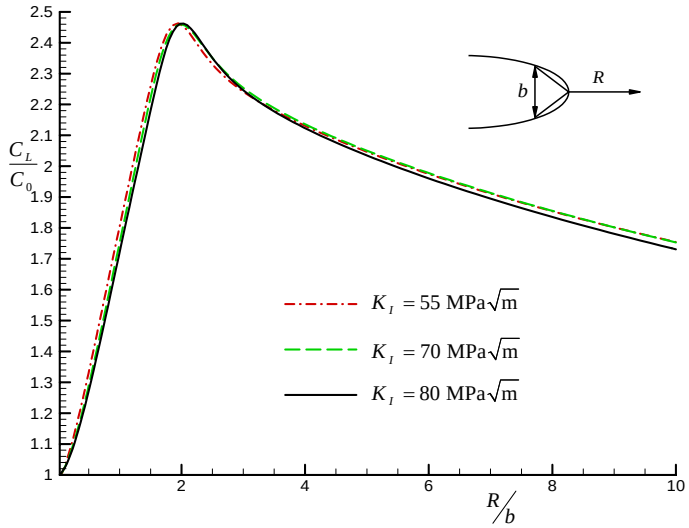

FIGURE 12: NORMALIZED HYDROGEN CONCENTRATION IN NILS C_L/C_0 VS NORMALIZED DISTANCE, R/b AHEAD OF THE CRACKED TIP AT $t = t_{ss} = 30$ days UNDER VARIOUS VALUES OF APPLIED STRESS INTENSITY FACTOR. THE DOMAIN SIZE IS $L = 14.3$mm .

Looking at the normalized hydrogen transport Eq. (10), one sees that there is no explicit dependence on the hydrogen diffusion coefficient *D*. Therefore, the non-dimensional time τ_{ss} to steady state is independend of *D*. Then by virtue of the definition of the non-dimensional time τ by Eq. (9), one concludes that

$$t_{ss} = \frac{f\left(L, \text{material parameters}\right)}{D}, \qquad (16)$$

where function f is independent of applied stress intensity and calculated equal to 5.184×10^{-5} m^2 specifically for the given material parameters and $L = 14.3$mm . The importance of Eq. (16) lies in the fact that if the domain geometry and all the material properties reported in Table 1 and used in the calculation remain the same except the diffusion coefficient which is reduced by a factor of 10 to $D = 2 \times 10^{-12}$ m^2/s, then the time to steady state increases by a factor of 10, that is, it becomes 300 days.

To examine the effect of the domain size parameter L on the steady state concentration profiles and time, additional transient hydrogen transport calculations were performed with L = 10.8, 14.3, 20.01, 30.8, 41.0, 49.6 and 60.0 mm under the same stress intensity factor of $K_I = 55$ MPa$\sqrt{\text{m}}$. For these domain sizes, t_{ss} values were found to be 15, 30, 50, 85, 115, 140 and 165 days, respectively. The plot of t_{ss} as a function of the domain size is shown in Fig. 13. The plot shows nearly a linear relation between t_{ss} and domain size in the range of 10-60 mm domain size. The NILS concentrations at time t_{ss} for different domain sizes are also plotted in Fig. 14. As the domain size gets larger, the peak value of the NILS concentration increases. However, Fig. 15 shows that the peak values of NILS concentration at t_{ss} tend to level at a value less than 2.6 as the domain size increases.

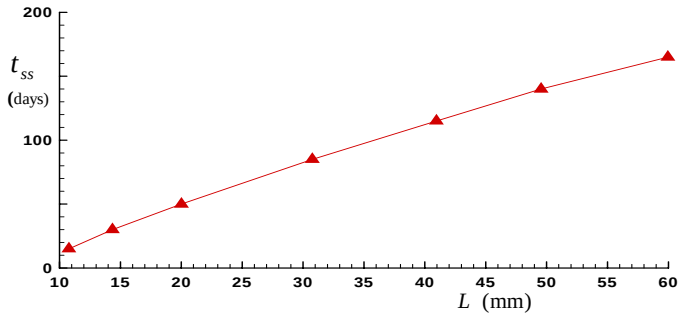

FIGURE 13: PLOT OF EFFECTIVE TIME TO STEADY STATE t_{ss} VS. DOMAIN SIZE L .

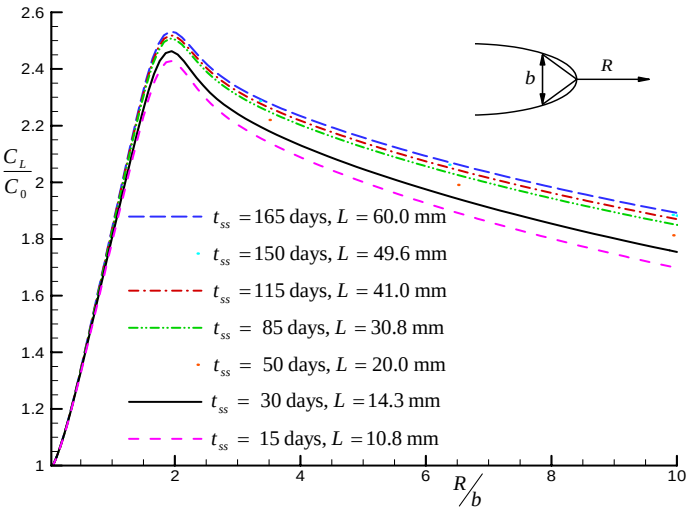

FIGURE 14: NORMALIZED HYDROGEN CONCENTRATION C_L/C_0 IN NILS AT $t = t_{ss}$ VS NORMALIZED DISTANCE R/b AHEAD OF THE CRACK TIP FOR DIFFERENT DOMAIN SIZES.

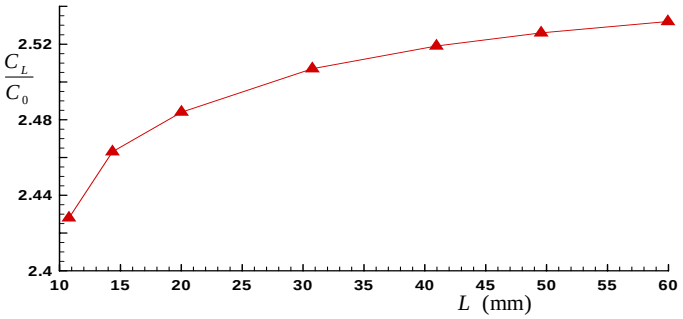

FIGURE 15: PLOT OF PEAK VALUES OF THE NORMALIZED HYDROGEN CONCENTRATION C_L/C_0 IN NILS AT $t = t_{ss}$ VS. DOMAIN SIZE L .

CONCLUDING REMARKS

The coupled transient hydrogen diffusion initial/boundary-value problem and the large strain elastoplastic boundary value problem were solved in the neighborhood of a blunting crack tip at a hydrogen gas environment using material properties for a pipeline steel. An effective time t_{ss} to steady state has been introduced. It denotes the time at which the NILS hydrogen concentration at the hydrostatic-stress peak location reaches 98% of the final steady state value. The effective time has been defined on the basis of the diffusible hydrogen which is the NILS populations. Once the NILS populations reach steady state so do the corresponding trapping ones as dictated by Eq. (1). The simulation results may be summarized as follows:

i) Under small scale yielding conditions, t_{ss} is independent of the applied stress intensity factor and is inversely proportional to the diffusion coefficient D as described by Eq. (16).

ii) The NILS concentration profile at steady state exhibits the same scaling features in terms of the applied stress intensity factor as the classical stress profile scales with load in the small scale yielding solution at a blunting crack tip.

iii) The magnitude of the peak NILS concentration at steady state is independent of the applied stress intensity factor, but depends on the domain size.

iv) The magnitude of the normalized peak NILS concentration at steady state seems to level at a value less than 2.60.

v) The effective time t_{ss} varies almost linearly with domain size.

Certainly the calculated time to steady state provides an upper bound to the time for embrittlement. Of course experimental evidence is required to discern the importance of hydrogen at NILS or trapping sites on triggering the degradation effect. Precise identification of the embrittlement conditions requires the coupling of the present simulations with a micromechanics model for fracture. Experimental work and theoretical calculations on fracture initiation ahead of a crack tip is the subject of ongoing research.

ACKNOWLEDGMENTS

The authors gratefully acknowledge support from DOE (Grant GO15045) and the National Science Foundation (Grant DMR 0302470).

REFERENCES

[1] Johnson, W. H., 1875, “On some remarkable changes produced in iron and steel by the action of hydrogen and acids,” In: C. D. Beachem, ed., *Proceedings of the Royal Society of London*, **23**.

[2] Hirth, J. P., 1980, “Effect of Hydrogen on The Properties of Iron and Steel,” *Metallurgical Transaction A*, **11A**, pp. 861-890.

[3] Birnbaum, H. K., Robertson, I. M., Sofronis, P., and Teter, D., 1997, “Mechanisms of Hydrogen related Fracture - a review,” In *Second International Conference on Corrosion Deformation Interactions*, CDI'96, Nice, Fracnce, 24-26 September, 1996, T. Magnin, ed.,. The institute of Materials, Great Britain, pp. 172-195.

[4] Thompson, A. W., 1977, “Materials For Hydrogen Service,” In *Hydrogen, its technology & Implications*, K. E. Cox and K. D. Williamson, eds., Vol. 2 Transmission and Storage, Cleveland, CRC Press, pp. 85-124.

[5] Birnbaum, H. K., 1977, “Hydrogen related failure mechanisms in metals,” In *Environmental Sensitive Fracture of Engineering Materials*, Z. A. Foroulis, ed., Proceedings of Symposium on Environmental Effects on Fracture, Chicago, Illinois, 24-26 October 1977, Warendale, PA: Metallurgical Socienty of AIME, pp. 326-360.

[6] Birnbaum, H. K., and Sofronis, P., 1994, “Hydrogen-enhanced localized plasticity - a mechanism for hydrogen related fracture,” *Material Science and Engineering A.*, **176**, pp. 191-202.

[7] Kitagawa, H., and Kojima, Y., 1983, “Diffusion of Hydrogen near an Elasto-Plastically Deformed Crack Tip,” In *Atomistic Fracture*, R.A. Latanision, and J. R. Pickens. eds., Proceedings of a NATO Advanced Research Institiute on Atomistics of Fracture, Calcatoggio, Corsica, France, 22-31 May, 1981, New York, Plenium Press, pp. 799-811.

[8] Sofronis, P., and McMeeking, R. M., 1989, “Numerical Analysis of Hydrogen Transport Near a Blunting Crack Tip,” *Journal of Mechanics and Physics of Solid*, **37**(3), pp. 317-350.

[9] Lufrano, J., and Sofronis, P., 1999, “Enhanced Hydrogen Concentration Ahead of Rounded Notches and Cracks - Competition Between Plastic Strain and Hydrogen Stress,” *Acta Materalia*, **46**(5), pp. 1519-1526.

[10] Krom, A. H. M., Koers, R. W. J., and Bakker, A., 1999, “Hydrogen Transport Near a Blunting Crack Tip,” *Journal of Mechanics and Physics of Solids*, **47**(4), pp. 971-992.

[11] Taha, A., and Sofronis, P., 2001, “A Micromechanics Approach to the Study of Hydrogen Transport and Embrittlement,” *Engineering Fracture Mechanics*, **68**(6), pp. 803-837.

[12] Dadfarnia, M., Sofronis, P., Robertson, I., Somerday, B. P. , Muralidharan, G. , and Stalheim. D., 2006, “Numerical simulation of hydrogen transport at a crack tip in a pipeline steel,” Proceedings of the IPC2006, 6th International Pipeline Conference, September 25-29, 2006, Calgary, Alberta, Canada.

[13] Peisl, H., 1978, “Lattice strains due to hydrogen in metals,” In *Hydrogen In Metals I, Topics in Applied Physics*, G. Alefeld and J. Volkl, eds., Vol. 28, New York, Springer, pp. 53-74.

[14] Robertson, I. M., 2001, “The effect of hydrogen on dislocation dynamics,” *Engineering Fracture Mechanics*, **68**(6), pp. 671-692.

[15] Oriani, R. A., 1970, "The Diffusion and Trapping of Hydrogen in Steel," *Acta Metallurgica*, **18**(1), pp. 147-157.
[16] Lufrano, J., Sofronis, P., and Symons, D., 1998, "Hydrogen Transport and Large Strain Elasto Plasticity Near a Notch in Alloy X-750," *Engineering Fracture Mechanics*, **59**(6), pp. 827-845.
[17] Irwin, G. R., 1960, Fracture Mechanics, In J. N. Goodier, and N. J. Hoff, eds., Structural Mechancis, *Proceedings of the First Symposium of Naval Structural Mechanics*, Standford University, pp. 557 - 594.
[18] Liang, Y., Sofronis, P., and Dodds, R. H., Jr., 2004, "Interaction of hydrogen with crack-tip plasticity:effects of constraint on void growth," *Materials Science and Engineering A*, **366**(2), pp. 397-411.
[19] Kumnick, A.J., and Johnson, H.H., 1980, "Deep Trapping States For Hydrogen in Deformed Iron," *Acta Materialia*, **28**(1), pp. 33-39.